

Vector Sensor Antenna Design for VHF Band

A. Musicant, B. Almog, N. Oxenfeld, and R. Shavit, *Senior Member, IEEE*

Abstract—A very high frequency (VHF) vector sensor antenna (VSA) composed of three small polygon orthogonal loops operating as three orthogonal electric dipoles and three orthogonal magnetic dipoles is designed and implemented. The VSA is used to estimate the angle of arrival (AoA) in azimuth and elevation of an incident electromagnetic (EM) signal by measuring its electric and magnetic field Cartesian components. The S-parameters (simulated and experimental) of the VSA and the AoA estimation results for different scenarios are presented. Furthermore, it is shown that the AoA performance is highly affected by the presence of a conductive platform in close vicinity of the VSA. The Cramer–Rao lower bound is derived for this case using the beam-former mathematical model.

Index Terms—Direction-of-arrival (DoA) estimation, magnetic sensors, unmanned aerial vehicles.

I. INTRODUCTION

PRACTICAL angle-of-arrival (AoA) estimation systems for the very high frequency (VHF) band are usually based on a large antenna array that collects data from several elements. A vector sensor antenna (VSA) system for AoA estimation has a major advantage over competing designs due to its simplicity and compact size, which enables high mobility.

The generalized VSA is composed of three collocated orthogonal electric dipoles and magnetic loops measuring the six Cartesian components of the electromagnetic (EM) field. By implementing the vector cross operator between the electric and magnetic fields, the Poynting vector and the wave propagation direction can be derived [1]. Since the introduction of the VSA concept some attempts to design and built such an antenna were made as described in [2]. Furthermore, calibration methods were established for the VSA mounted on different platforms and are presented in [3]. The major challenges of the construction of a small VSA like the one required for VHF band are implementation of the collocated electric and magnetic sensors, achieving low coupling between its different elements, and reaching the required sensitivity over a wide frequency band.

In this letter, a unique implementation accompanied by simulation and measured results of the proposed VSA for the VHF band is presented. The design considerations are discussed in Section II. The AoA analysis performance is presented in Section III. The well-known mathematical model of the beam forming is adjusted using the normalized steering matrix to the estimation problem of the VSA and is described

Manuscript received December 31, 2014; revised February 22, 2015; accepted March 01, 2015. Date of publication March 06, 2015; date of current version June 22, 2015.

A. Musicant and R. Shavit are with the Department of Electrical and Computer Engineering, Ben-Gurion University of the Negev, Beer-Sheva 84105, Israel (e-mail: amirmusi@post.bgu.ac.il; rshavit@ee.bgu.ac.il).

B. Almog and N. Oxenfeld are with Elta Electronic Industries Ltd., Ashdod 77102, Israel.

Color versions of one or more of the figures in this letter are available online at <http://ieeexplore.ieee.org>.

Digital Object Identifier 10.1109/LAWP.2015.2409315

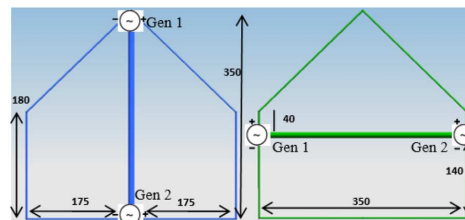


Fig. 1. Geometry of the VSA loops (all dimensions are in mm).

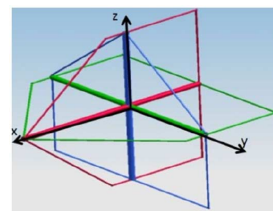


Fig. 2. Model of the constructed VSA.

in Section IV. The presence of a conductive platform in close vicinity of the antenna has a major effect on the antenna pattern and its steering matrix. The Cramer–Rao lower bound (CRLB) [4, Ch. 33, Sec. 3], [5] is derived for this case and compared to the CRLB of the antenna in free space.

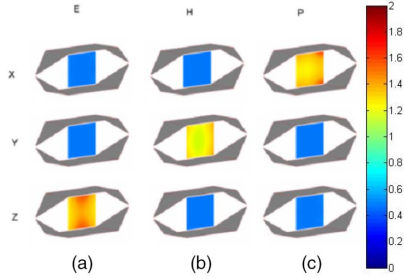
II. IMPLEMENTATION AND MEASURED RESULTS

A well-known electrically small antenna loop, which acts as an electric dipole and as a magnetic dipole, is the opposing loads loop (OLL) described in [6]. The major advantage of this loop design is that it can perform as an electric dipole and as a magnetic dipole by switching between two loop configurations. This feature reduces the required number of elements of the VSA to three collocated loops instead of six collocated elements (three electric dipoles and three magnetic dipoles). This feature is obtained by adding or subtracting the voltages induced on the two opposite loads of the loop element. In the following, they will be addressed as electric mode and magnetic mode. This antenna element is usually utilized in near-field sensor applications to probe the complex structure of the EM fields components.

For the VSA applications it is necessary to sense both the electric and magnetic fields in order to derive the AoA. Thus, the OLL is an attractive candidate for implementing electric and magnetic dipoles in the construction of the VSA. The proposed VSA includes three orthogonal collocated polygon OLLs. Accordingly, there are six loads in the system. Two types of polygon loops were used, as shown in Fig. 1, to implement the required three loops. The whole VSA model is shown in Fig. 2. The loop's pentagonal shape was chosen due to aerodynamic considerations. The solid thick line indicates the symmetry line of the closed loop and the location of the loads. The symmetry line divides the loop to two equal area and circumference polygons. The dimensions are tuned to achieve the required sensitivity while preserving the small dipole pattern characteristics.



Fig. 3. Picture of the TEM cell.

Fig. 4. TEM cell near-field amplitude distribution. (a) Electric field magnitude in the z direction [2 V/m]. (b) Magnetic field magnitude in the y direction and [mA/m]. (c) Poynting flux magnitude in x direction [mW/m²].

The electric mode is generated by exciting the two generators in phase and the magnetic mode is generated by exciting the two generators out of phase.

The antenna was modeled and simulated using the commercial EM software WIPL-D (wires, plates, and dielectrics) based on method of moments (MoM) solution. The model was tested in a specially built transverse EM (TEM) cell. The measurements were made from 20 to 100 MHz. The general TEM cell view is captured in Fig. 3. The cell dimensions are 1×1 m and approximately 3 m long. The TEM cell simulates the attributes of a far field as shown in Fig. 4. Low mutual coupling among the elements in the VSA is essential to the accuracy of the mathematical model discussed in Section III. It is known [6] that the OLL exhibits low coupling between its electric and magnetic modes, and therefore it was chosen for the implementation. Fig. 5 shows a comparison between the measured and simulated mutual coupling S_{12} between the two operational modes (electric and magnetic) for the loop in the X - Y plane. Due to the high sensitivity of the mutual coupling to unavoidable fabrication errors in the loops dimensions, an 0.5% defects in the line lengths and loads positions was inserted to the simulation. In this case very good agreement was obtained between the measured and simulated data for OLL with defects. The measured coupling is less than -30 dB in the 20–100 MHz frequency band. Simulated mutual coupling S_{12} of two orthogonal collocated OLLs excited in different modes is given in Fig. 6. One can observe that the mutual coupling between any modes configurations is less than -45 dB. The reflection coefficient S_{11} of the OLL is shown in Fig. 7 in dB ($S_{11}[\text{dB}] = 20 \log_{10}(S_{11})$). Note that the simulation S_{11} results does not include the feeding lines and the baluns used for matching, and yet it shows a very good agreement with the measured data.

The signal model used for the estimation problem is the common form used for spatial signal processing. The assumptions made are that the signal \mathbf{S}_n is narrow band with unknown amplitude while the noise is additive. The model assumed is

$$\begin{bmatrix} \mathbf{E}_n \\ \mathbf{H}_n \end{bmatrix} = \mathbf{A}(\phi, \theta, \tau, \gamma) \mathbf{S}_n + \mathbf{w}_n \quad (1)$$

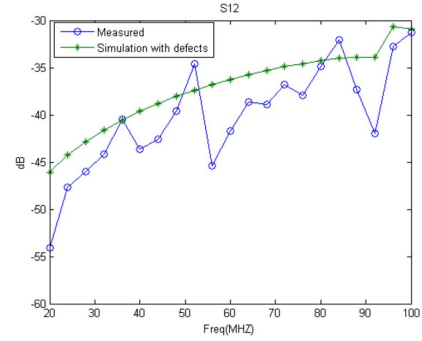
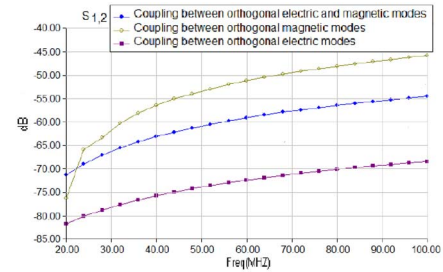
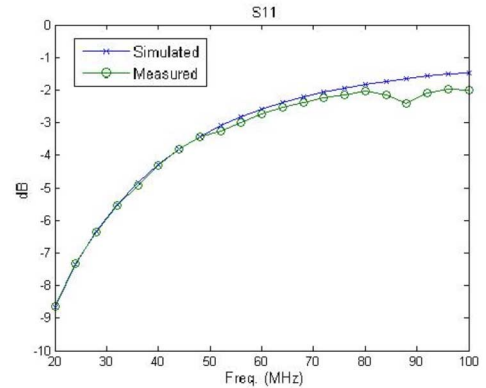
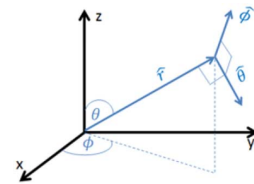
Fig. 5. Mutual coupling between electric and magnetic modes for a loop in the X - Y plane.Fig. 6. Simulated mutual coupling S_{12} between orthogonal modes.Fig. 7. Reflection coefficient S_{11} [dB] as a function of frequency.

Fig. 8. Coordinate system and its parameters.

where ϕ and θ are the azimuth and elevation angles (i.e., Fig. 8) while γ is the phase difference between the electric field components E_ϕ and E_θ . $\tan \tau$ is the ratio between the amplitudes of the electric field in ϕ direction and θ direction (i.e., $\tan \tau = |E_\phi/E_\theta|$) and \mathbf{w}_n is the additive noise. \mathbf{E}_n and \mathbf{H}_n are the n sample of the electric and magnetic field vectors while \mathbf{A} is the normalized steering matrix. The transmitted signal \mathbf{S}_n is a deterministic signal with unknown amplitude. This is a reasonable assumption for narrow band signals and is a good test case due to the existence of an analytic solution. For higher accuracy one can assume that the signal is unknown and increase the computation complexity.

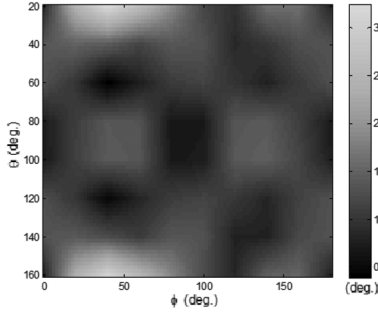


Fig. 9. Average AoA error.

For the free-space case the steering matrix \mathbf{A} is given by [1]

$$\mathbf{A}(\phi, \theta, \tau, \gamma) = \begin{bmatrix} \cos \phi \cos \theta & -\sin \phi \\ \sin \phi \cos \theta & \cos \phi \\ -\sin \theta & 0 \\ -\sin \phi & -\cos \phi \cos \theta \\ \cos \phi & -\sin \phi \cos \theta \\ 0 & \sin \theta \end{bmatrix} \begin{bmatrix} \sin \tau e^{j\gamma} \\ \cos \tau \end{bmatrix}. \quad (2)$$

The steering matrix as shown in (2) assumes that there is no mutual coupling between the VSA elements; thus, in order for the mathematical model to hold low mutual coupling is essential. Making the assumption of very low mutual coupling based on the results presented in Figs. 5 and 6, an experiment was made to determine the theoretical error of the VSA in a noise-free environment (i.e., $\mathbf{w}_n = 0$). The VSA was illuminated by plane waves at different AoAs. The azimuth angle (ϕ) and the elevation angle (θ) were evaluated directly from the Poynting vector cross operator product (\underline{s}) of the electric and magnetic vectors measured by the VSA and given by

$$\underline{s} = s_x \hat{x} + s_y \hat{y} + s_z \hat{z} = \frac{1}{2} \underline{E} \times \underline{H}^*. \quad (3)$$

From (3), the estimated elevation and azimuth angles (θ_{est} , ϕ_{est}) can be evaluated by

$$\theta_{est} = \tan^{-1}(\sqrt{s_x^2 + s_y^2}/s_z); \phi_{est} = \tan^{-1}(s_x/s_y). \quad (4)$$

The measured RMS error defined as $((\theta_{est} - \theta)^2 + (\phi_{est} - \phi)^2)^{1/2}$ is shown in Fig. 9. Spline interpolation was used to determine the AoA RMS error with 2° resolution. Note that the error presented is due to direct calculation using the theoretical steering matrix \mathbf{A} with no calibration. The good results testify that the mathematical model holds.

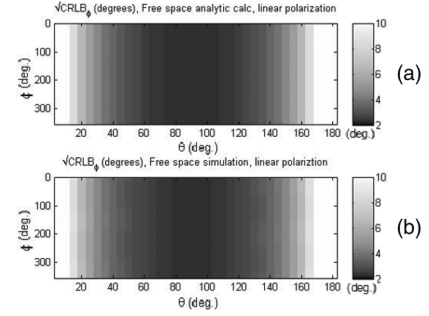
III. AOA PERFORMANCE ANALYSIS

Most antenna studies analyze the antenna attributes which determine the signal-to-noise ratio (SNR). In this letter, we assume that the SNR is known and analyze the estimation performance of the AoA using the CRLB for a specified mathematical model. The CRLB bounds the variance for any unbiased estimator from below; thus its minimization is required.

In the free-space case modeled by (1) and (2) the CRLB can be derived analytically for Gaussian noise (\mathbf{w}_n) with no correlation. Thus, in mathematical notation

$$\mathbf{w}_n \sim \mathbf{N}_c(0, \mathbf{R}); \mathbf{R} = |\sigma|^2 \mathbf{I} \quad (5)$$

where \mathbf{R} is the autocorrelation matrix, \mathbf{I} is the $N \times N$ identity matrix with N samples and σ is a complex scalar, \mathbf{N}_c denotes

Fig. 10. $CRLB_\phi$ estimation for (a) analytic computation and (b) computation based on WIPL-D simulation data.

the normal complex distribution. Thus, the distribution of the EM fields is also normal complex given by

$$\begin{bmatrix} \mathbf{E}_n \\ \mathbf{H}_n \end{bmatrix} \sim \mathbf{N}_c(\mathbf{A}(\phi, \theta, \tau, \gamma) \mathbf{S}_n, \mathbf{R}). \quad (6)$$

From (6) it is easy to compute the Fisher information matrix (FIM). First, we define the SNR and the unknown vector (ψ).

$$\psi = [\theta, \phi, \tau, \gamma]^T; \mathbf{SNR} = \frac{\sum_{n=0}^{N-1} |\mathbf{S}_n|^2}{N|\sigma|^2}. \quad (7)$$

Thus the **FIM** becomes

$$\mathbf{FIM} = N * \mathbf{SNR} \begin{bmatrix} 1 & 0 & 0 & 0 \\ 0 & 1 + \cos^2 \theta & -2 \cos \theta \cos \gamma & \cos \theta \sin 2\tau \sin \gamma \\ 0 & -2 \cos \theta \cos \gamma & 2 & 0 \\ 0 & \cos \theta \sin 2\tau \sin \gamma & 0 & 2 \sin^2 \tau \end{bmatrix}. \quad (8)$$

Finally by inverting the **FIM** the CRLB is derived

$$CRLB_\theta = \frac{1}{N * \mathbf{SNR}} \\ CRLB_\phi = \frac{1}{N * \mathbf{SNR} * (1 + \cos^2 \theta - 2 \cos^2 \theta (\cos^2 \gamma + \cos^2 \tau \sin^2 \gamma))} \quad (9)$$

where N is the number of samples. The CRLB for azimuth angle estimation and linear polarization (i.e., $\gamma = 0$) is reduced to

$$CRLB_\phi = \frac{1}{N * \mathbf{SNR} * \sin^2 \theta}. \quad (10)$$

Similarly, for circular polarization (i.e., $\tau = \pi/4, \gamma = \pi/2$) is

$$CRLB_\phi = \frac{1}{N * \mathbf{SNR}}. \quad (11)$$

Notice that from (11) it is seen that a phase difference in the electric field components improves the AoA estimate and for circular polarization it eliminates the dependence of the CRLB on the elevation angle θ . That is due to the fact that if there is no phase difference, ϕ and τ cannot be separated for $\theta = \{0, 180\}$. The CRLB for azimuth angle in free-space case is shown in Fig. 10 for $N = 64$ and $\text{SNR} = 10$ dB at 60 MHz compared to the analytic solution. The computation is based on WIPL-D simulations. The results shown in Fig. 10 are in very good agreement. The $CRLB_\theta$ is constant and equal to $1.5625 * 10^{-3} (\text{rad}^2)$.

The radiation patterns of antennas are affected by the platform on which they are usually mounted on. To determine the effect of a platform on the VSA performance, the VSA was positioned in close vicinity to a platform, simulated by a perfect electric conductor (PEC) cylinder as shown in Fig. 11. The effect of the platform was evaluated by computing the VSA's CRLB of the

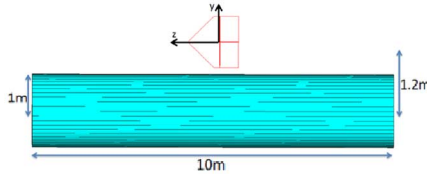
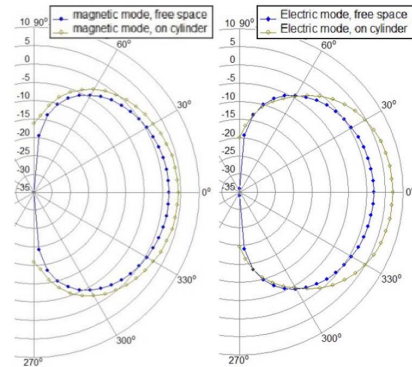


Fig. 11. Geometry of the VSA on a cylindrical platform.

Fig. 12. VSA radiation patterns in the y - z plane ($\phi = 90^\circ$) with and without the PEC cylinder presence.

AoA relative to the free-space case. The cylinder was chosen for practical reasons to approximate an arbitrary fuselage.

The cylinder introduces distortion to the EM fields in all orientations of the VSA. As an example of the expected pattern distortion Fig. 12 shows a comparison in the radiation patterns in the E-plane (Y - Z plane) for $\phi = 90^\circ$ with and without the cylindrical platform at 60 MHz.

From Fig. 12 it is clear that the steering matrix from the free-space case does not hold. Thus, the new steering matrix was derived numerically from the simulated pattern data. The simulated normalized CRLB for azimuth and elevation AoA for vertical and horizontal polarizations of the VSA on a cylindrical platform are shown in Figs. 13 and 14, respectively. The data are presented in dB and normalized to the free-space CRLB

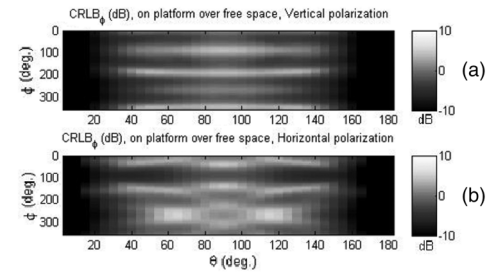
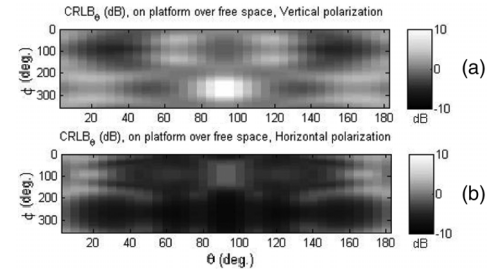
$$CRLB_{\phi/\theta}[dB] = 10 * \log \frac{CRLB_{\phi/\theta} |_{test\ case} [deg]}{CRLB_{\phi/\theta} |_{free\ space} [deg]}, \quad (12)$$

In this measure, high figures mean that the estimation performance deteriorates and vice versa.

Note (i.e., Fig. 11) that the center of the cylinder is located at $\phi = 270^\circ$ relative to the VSA axis and that the cylinder's main axis is parallel to the VSA's z axis. The N and SNR values are the same as in the free-space case, and the frequency is 60 MHz.

One can observe that the radiation pattern distortions in the case of the cylindrical platform affect severely the estimation performance, especially the $CRLB_{\theta}[dB]$. The degradation of $CRLB_{\theta}[dB]$, for most angles, is increased by 3 dB. Furthermore, it is seen that the azimuth estimation is more vulnerable to waves in horizontal polarization and the elevation estimation is more sensitive to vertical polarization. It can as well be seen that the diffraction which occurs for vertical polarization in elevation angles of 5° and 175° and azimuth angles 215° to 325° introduce degradation of the elevation estimate.

In order to improve the CRLB, besides increasing the number of samples or SNR, one should try to place the VSA on the platform in such a manner that the elements preserve their dipole like pattern or where the EM fields behaves like a plane wave, and it is recommended to avoid diffraction effects.

Fig. 13. Normalized $CRLB_{\phi}$ estimation for the VSA on a cylindrical platform and two orthogonal polarizations. (a) Vertical Polarization. (b) Horizontal polarization.Fig. 14. Normalized $CRLB_{\theta}$ estimation for the VSA on a cylindrical platform and two orthogonal polarizations. (a) Vertical polarization. (b) Horizontal polarization.

IV. CONCLUSION

This letter describes the design, implementation, and performance analysis of a new VSA element used for AoA estimation in the VHF band. The CRLB of the AoA estimation by the VSA in the presence of an electrically large metal cylinder was derived and compared to the free-space case. A degradation in the estimation performance was identified due to the pattern distortion. One can expect that for more complicated platforms than the cylinder more erratic distortions are introduced to the antenna pattern. In these cases it is expected that the CRLB will be higher for larger angular sectors. Careful choice of the VSA location can reduce the radiation pattern distortions, but that cannot always be achieved; and in these cases calibration methods are needed [3]. The VSA is highly sensitive to the radiation pattern distortion compared to other DF systems, and thus it is important to carefully plane its location on the platform on which it is mounted. Additional improvement in the CRLB might be achievable by including the preferences of the scattered EM field, and this is a case for further study.

REFERENCES

- [1] A. Nehorai and E. Paldi, "Vector-sensor array processing for electromagnetic source localization," *IEEE Trans. Signal Process.*, vol. 42, no. 2, pp. 376–398, Feb. 1994.
- [2] L. Lo Monte, B. Elnour, and D. Erricolo, "Distributed 6D vector antennas design for direction of arrival applications," in *Proc. Int. Conf. Electromagn. Adv. Appl.*, 2007, pp. 431–434.
- [3] S. Appadwedula and C. M. Keller, "Direction-finding results for a vector sensor antenna on a small UAV," in *Proc. 4th IEEE Workshop Sensor Array Multichannel Process.*, 2006, pp. 74–78.
- [4] H. Cramér, "Methods of estimation," in *Mathematical Methods of Statistics*. Princeton, NJ, USA: Princeton Univ. Press, 1999.
- [5] C. Radhakrishna Rao, "Information and the accuracy attainable in the estimation of statistical parameters," *Bull. Calcutta Math. Soc.*, vol. 37, pp. 81–89, 1945.
- [6] M. Kanda, "An electromagnetic near-field sensor for simultaneous electric and magnetic-field measurements," *IEEE Trans. Electromagn. Compat.*, vol. EMC-26, no. 3, pp. 102–110, 1984.